Moduli Spaces of Morse Functions for Persistence

Michael J. Catanzaro · Justin M. Curry · Brittany Terese Fasy · Jānis Lazovskis · Greg Malen · Hans Riess · Bei Wang · Matthew Zabka

Abstract We consider different notions of equivalence for Morse functions on the sphere in the context of persistent homology and introduce new invariants to study these equivalence classes. These new invariants are as simple—but more discerning than—existing topological invariants, such as persistence barcodes and Reeb graphs. We give a method to relate any two Morse–Smale vector fields on the sphere by a sequence of fundamental moves by considering graph-equivalent Morse functions. We also explore the combinatorially rich world of height-equivalent Morse functions, considered as height functions of embedded spheres in $\mathbb{R}^3$. Their level set invariant, a poset generated by nested disks and annuli from level sets, gives insight into the moduli space of Morse functions sharing the same persistence barcode.

M.J. Catanzaro
Iowa State University, E-mail: mjcatanz@iastate.edu

J.M. Curry
University at Albany SUNY, E-mail: jmcurry@albany.edu

B.T. Fasy
Montana State University, E-mail: brittany.fasy@montana.edu

J. Lazovskis
University of Aberdeen, E-mail: janis.lazovskis@abdn.ac.uk

G. Malen
Duke University, E-mail: gmalen@math.duke.edu

H. Riess
University of Pennsylvania, E-mail: hmr@seas.upenn.edu

B. Wang
University of Utah, E-mail: beiwang@sci.utah.edu

M. Zabka
Southwest Minnesota State University, E-mail: Matthew.Zabka@smsu.edu

1 Introduction

Morse theory describes the topology of a manifold $\mathbb{M}$ by studying well-behaved functions $f : \mathbb{M} \to \mathbb{R}$ (Milnor, 1963). This *well-behavedness* is qualified by the notion of a *Morse function*: a smooth real-valued function with no degenerate critical points. One of the main ideas of Morse theory is to associate the topological changes of the sublevel sets $\mathbb{M}_a = f^{-1}(\infty, a]$, as a varies, with the critical points of f. From an algebraic perspective, Morse functions are *effective* in topological problems due to their local rigidity; that is, critical points of Morse functions have a very simple local, quadratic structure (up to a change of coordinates) (Nicolaescu, 2007). From a homological perspective, the relationship between the topology of $\mathbb{M}$ and the critical points of f is described by the powerful Morse inequalities, which have both topological and geometric significance.
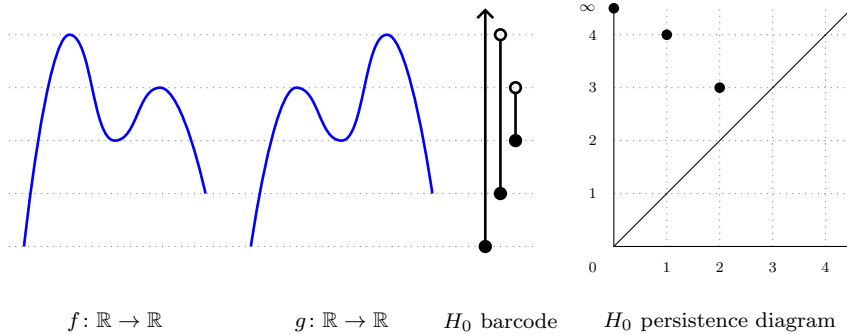

| $f : \mathbb{R} \to \mathbb{R}$ | $g : \mathbb{R} \to \mathbb{R}$ | H_0 barcode | H_0 persistence diagram |

Fig. 1 The graphs of two different functions $f, g : \mathbb{R} \to \mathbb{R}$ restricted to a finite interval in $\mathbb{R}$, and their identical one-dimensional barcode and persistence diagram based on sublevel set filtration. The longest bar in the barcode captures the connected component; while the 2nd longest bar is created due to the boundary condition.

Persistent homology is a relatively new tool for discriminating functions on topological spaces based on how the shape of their (sub)level sets evolve. In the standard setting, persistence is an extension of Morse theory, as it studies homology groups of sublevel sets connected by inclusion maps, $\mathbb{M}_a \hookrightarrow \mathbb{M}_b$ (for $a \leq b$). The evolution of shape is captured by what is known as the *persistence diagram* or *barcode* (Edelsbrunner and Harer, 2010; Ghrist, 2008). Barcodes enjoy properties such as *simplicity*, as a barcode is simply a collection of intervals in the real line; and *stability*, as small perturbations of shape produce small perturbations of the barcode. Both of these properties make persistence an ideal tool for studying the shape of data, with wide applications to science and engineering; see Edelsbrunner and Morozov (2012) for a survey.

We are interested in exploring different moduli spaces of Morse functions from the perspective of persistence. We characterize the set of Morse functions that give rise to the same barcode, see Figure 1 for an example. Some of these functions should be considered as different, because taking one function to another requires a significant deformation. In other words, we are putting different equivalence relations on the space of Morse functions that respect persistence, i.e., two functions can only be deemed equivalent only if they have the same barcode, but simply having the same barcode does not guarantee equivalence. Each choice of equivalence relation leads to a different moduli space structure on the space of Morse functions; and each equivalence class has an interesting combinatorial structure that can be used practically to enrich the barcode.

Instead of focusing on *any* Morse function $f \colon \mathbb{M} \to \mathbb{R}$, we are initially motivated by a simpler question by considering $\mathbb{M} = \mathbb{S}^2$: *How many Morse functions on the sphere $\mathbb{S}^2$ have the same barcode?* Or more precisely: *How many equivalence classes of Morse functions on the sphere have the same barcode?* Asking such an open question is a first step towards exploring three areas of interests described below. For simplicity, we sometimes require more from f, such as factoring as an embedding into Euclidean space followed by a projection, so as to exclude pathological examples like the Alexander horned sphere.

Topological data analysis: The simplicity of the barcode is both a benefit and a drawback, as information about the space and function is lost during its computation. Precisely how much information is lost? How does the barcode compare to other topological invariants, and does it fail to capture some key topological and geometric features? How does the analysis on a sphere extend to a compact surface of genus g? From a statistical perspective, how common is a particular barcode, and which one should we expect in a *general* situation?

Shape analysis: Properties of shapes, such as being convex, nested, elongated, or circular, are mostly geometric in nature. Do the discriminative capabilities of persistence—known to be mostly topological—also capture these geometric properties? Recent work by Bubenik et al. (2020) has shown that short intervals in barcodes encode geometric information; in particular, persistent homology detects the curvature of disks from which points are sampled. How much geometric information is preserved by the barcodes?

Topological descriptors, such as Reeb graphs (Reeb, 1946) and Morse–Smale complexes (Edelsbrunner et al., 2003a,b), provide an abstract and compact representation of data modeled by Morse functions. For instance, the small number of cells in a Morse–Smale complex can significantly reduce the number of cells when discretizing a shape, while keeping the same topological properties. Does persistence allow us to reduce the carried data even further?

We refer the interested reader to the survey paper by Biasotti et al. (2008) for a summary of shape analysis's relationship to persistence and Reeb graphs.

Dynamical systems: What is the space of all Morse or Morse–Smale vector fields, with and without the requirement of identical persistence as a

constraint? Equivalence classes of Morse–Smale vector fields on 2-manifolds have been studied previously (Peixoto, 1973; Fleitas, 1975; Gutierrez and de Melo, 1977); however, not in the context of persistence. It is known that the set of Morse–Smale vector fields on orientable surfaces is dense (Palis and de Melo, 1982, Theorem 2.6). Given two Morse–Smale vector fields which are not topologically equivalent, can we derive a distance measure between them? What is the minimal number of operations (critical pair cancellation or reverse-cancellation) to transform one to another?

1.1 Research Objectives

Our overarching goal is to classify and algorithmically construct all equivalence classes of Morse functions on a manifold, where the equivalence is captured by functions, embeddings, or dynamics, using barcodes as constraints. Fixing a homology degree, the *persistence map* is the map that takes a function f on $\mathbb{M}$ to its associated barcode (Curry, 2018). We classify the image, preimage, and embeddings of the preimage of the persistence map under different notions of equivalence relations. While there have been approaches to interpreting the persistence map functorially (Bauer and Lesnick, 2015; De Silva et al., 2016), and such categorical generalizations are of interest to us (see Section 4), considering the persistence map simply as a map rather than a functor does not take away from our analysis.

Let $\mathbb{M}$ denote a smooth manifold, and let $f \colon \mathbb{M} \to \mathbb{R}$ denote a Morse function. In this paper, we focus on characterizing Morse functions on the sphere $\mathbb{M} = \mathbb{S}^2$ that produce the same barcode.

- **Objective 1: Classifying the image.** Fix $\mathbb{M}$ (for example, $\mathbb{S}^2$) and the number and type of critical points that respect the Euler characteristic (for example, two maxima, one saddle point, and one minimum on $\mathbb{S}^2$). Enumerate the barcodes that correspond to sublevel set filtrations of functions $f \colon \mathbb{M} \to \mathbb{R}$. This is a computational objective, and can be interpreted by counting Morse–Smale graphs (Section 2) via elementary moves (Section 3) instead of functions. In this setting, we declare that two Morse functions $f, g \colon \mathbb{M} \to \mathbb{R}$ are *indistinguishable* if they are *graph equivalent* (Section 2).
- **Objective 2: Classifying embeddings of the preimage.** Fix $\mathbb{M}$ and a barcode, and ask how many different embeddings $\iota : \mathbb{M} \to \mathbb{R}^d$ of the space $\mathbb{M}$ into Euclidean space $\mathbb{R}^d$ produce the given barcode when projected onto a fixed axis via $\pi \colon \mathbb{R}^d \to \mathbb{R}$. In other words, we study the behavior of the function $f := \pi \circ \iota$. This is related to the persistent homology transform (Turner et al., 2014), which asks the same question, but for all directions. Here, two Morse functions $f, g : \mathbb{M} \to \mathbb{R}$ (where $f := \pi \circ \iota$ and $g := \pi \circ \iota'$) are considered *indistinguishable* if (i) they generate the same barcode and (ii) they are *poset equivalent* (Section 2).
- **Objective 3: Classifying the preimage.** Fix $\mathbb{M}$ and a barcode, and ask for all functions, up to *level-set preserving equivalence*, whose image is the given barcode. This topological objective benefits from the Reeb

graph (Reeb, 1946), which enriches the barcode by distinguishing different type of persistence pairings, and its refinement the *decorated Morse–Smale graph*, introduced in Section 2.1. Two Morse functions $f, g \colon \mathbb{M} \to \mathbb{R}$ are *indistinguishable* in this context if (i) they generate the same barcode and (ii) they give rise to isomorphic decorated Morse–Smale graphs.

Classifying Morse functions under different notions of equivalences via the persistence map is well-motivated, as persistence has emerged as a central tool of topological data analysis. Applications of persistence include shape analysis (Carlsson et al., 2004; Poulenard et al., 2018), cancer research (Seemann et al., 2012; Lockwood and Krishnamoorthy, 2015; Hofmann et al., 2018; Qaiser et al., 2019) and material sciences (Lee et al., 2018). By exploring the above moduli spaces, we aim to build a better or enriched barcode for real-world applications.

1.2 Related Work

The mathematical study of height functions through level sets (contour lines) and relationships between them dates back to at least the 1850s, when Cayley classified topographical maps based on configurations of contour lines (Cayley, 1859). Maxwell (1870) extended this work and laid the foundation for Morse theory. Reeb (1946) defined a graphical invariants to classify Morse functions; today, we call this invariant the *Reeb graph*. Later, Arnold (1991, 1992) defined geometric equivalence classes of functions on $\mathbb{S}^1$ using a notion of "snakes". The classification for functions on surfaces is much more involved, and has been considered in certain cases (Arnold, 2007; Nicolaescu, 2007), the latter of which analyzed homological and geometric equivalence of Morse functions on $\mathbb{S}^2$. Further, Kulinich (1998) and Sharko (1996, 2003) classified Morse functions on surfaces, up to geometric equivalence, using Reeb graphs. Reeb graphs use level-sets of functions, and the analogous join tree or merge tree structure with sublevel sets was developed by Pascucci and Cole-McLaughlin (2004) and Curry (2018). Further implications of Reeb graphs for persistent homology were considered by Di Fabio and Landi (2016); Bauer et al. (2018).

From the dynamical system perspective, Peixoto (1973) classified Morse–Smale flows on two-manifolds up to trajectory topological equivalence using the concept of "distinguished graph". Subsequent work by Fleitas (1975) and Wang (1990) gave simpler invariants for Morse flows on two-manifolds. Oshemkov and Sharko (1998) also considered the problem of topological trajectory classification of Morse–Smale flows on closed surfaces and introduced a "three-color graph" as another alternative to the Peixoto invariant. Morse flows are also used to determine two-dimensional Hamiltonian flows; and Sakajo and Yokoyama (2018) developed tree representations for such flows. Both three-color graphs and tree representations are combinatorial codings that detail processes for constructing a flow by adding pairs of critical points. Finally, Adams and Carlsson (2015) used topological arguments like the ones in Section 4 to decompose spaces for network evasion paths, however they did

not use the language of Morse functions. Our work focuses on invariants based on cell decompositions of the domain using gradient flows. It is primarily concerned with the structure of the Morse–Smale complex and its interplay with persistence, which is distinct from previous approaches.

The formal underpinnings of the sequence of moves described in Section 3 originate from Cerf theory (also known as pseudoisotopy theory) (Cerf, 1970; Hatcher and Wagoner, 1973). In proving his celebrated "Pseudoisotopy Theorem", Cerf described the low codimension strata of a particular stratification on the space of smooth functions on a smooth compact manifold. The codimension-zero stratum consists of Morse functions with distinct critical values, and the codimension-one stratum consists of either 'generalized Morse functions' (those with a single cubic 'birth-death' singularity), or Morse functions with precisely two critical values equal. Furthermore, Cerf showed that a generic or typical path of smooth functions lies in the codimension-zero stratum for all but finitely many 'times' (thinking of the path parameter as 'time'), at which points the function lies in the codimension-one stratum. The moves described in Section 3 are inspired by moving across the codimension-one stratum in the space of smooth functions and passing through a generalized Morse function. The statement and proof of Theorem 3 relies on this description of the stratification and adapts these ideas to the combinatorics of the Morse–Smale graph of a surface.

Performing one of the moves introduced in Section 3 can be thought of as a perturbation of the initial Morse-Smale flow (albeit a fairly large one from the perspective the aforementioned stratification of Cerf). Perturbations in the space of all vector fields have been studied by other authors (see Szymczak (2012) and its extensive references). This perspective might be useful for future work, but we do not take this approach now.

1.3 Overview

Our main contributions in this paper are:

– New notions of equivalence among (embeddings of) Morse functions containing persistence information;
– A set of fundamental operations on Morse–Smale vector fields that relate all such vector fields;
– A foundation for counting the number of Morse functions producing the same barcode.

In Section 2.1 we begin with a background to the functions of interest in the context of persistent homology, with new and existing notions of equivalence among these functions in Section 2.2. Section 3 contains a method for relating Morse–Smale vector fields on the sphere, building from existing decomposition results (Edelsbrunner et al., 2003b). Section 4 explores one of the new invariants, the nesting poset, and describes a zigzag poset structure in Corollary 1, making steps to extend it combinatorially in Conjecture 1, with

a goal of developing an enriched barcode. Section 5 presents a lower bound in Conjecture 2 to counting height-equivalence classes of Morse functions that factor through $\mathbb{R}^3$ as smooth embeddings, which leads to better understanding of Morse functions by their barcode.

2 Technical Background

We first summarize relevant aspects of Morse theory, see Milnor (1963), Matsumoto (1997), and Nicolaescu (2007) for detailed expositions on the topic. We then review known notions of equivalence among Morse functions. After that, we introduce the notions of graph equivalence, height equivalence, and poset equivalence. We conclude by a comparison of equivalence relations among Morse functions.

2.1 Morse Functions and Persistence

Let $\mathbb{M}$ be a smooth, compact, orientable manifold, equipped with a Riemannian metric $g_{\mathbb{M}}$, and $f \colon \mathbb{M} \to \mathbb{R}$ be a smooth function.

2.1.1 Morse Functions

A critical point p of $\mathbb{M}$ is *non-degenerate* if there exists a chart $(x_1, \ldots, x_n)$ on a neighborhood U of p such that

1. $x_i(p) = 0$ for all i, and
2. $f(x) = f(p) - x_1^2 - \cdots - x_\lambda^2 + x_{\lambda+1}^2 + \cdots + x_n^2$.

The number λ is the *(Morse) index* of the critical point p, and is independent of the choice of chart. The index of a critical point is an integer between 0 and the dimension of $\mathbb{M}$. A smooth function $f \colon \mathbb{M} \to \mathbb{R}$ is a *Morse function* if all its critical points are non-degenerate. Furthermore, f is an *excellent Morse function* if all critical points have distinct function values (Nicolaescu, 2008). All Morse functions considered in this paper are excellent, and referred to simply as Morse functions.

2.1.2 Handle Decomposition

For $f \colon \mathbb{M} \to \mathbb{R}$ a Morse function, let $\mathbb{M}_t := f^{-1}(-\infty, t] = \{x \in \mathbb{M} \mid f(x) \leq t\}$ denote sublevel sets of f. Morse theory studies how $\mathbb{M}_t$ changes as the parameter t changes. There are two fundamental theorems regarding handle decomposition of manifolds in Morse theory (Milnor, 1963; Matsumoto, 1997; Nicolaescu, 2007).

Theorem 1 ((Milnor, 1963, Theorem 3.1)) *If f has no critical values in the real interval $[a, b]$, then $\mathbb{M}_a$ and $\mathbb{M}_b$ are diffeomorphic.*

Theorem 2 ((Milnor, 1963, Theorem 3.2),(Matsumoto, 1997, page 77)) *Let p be a critical point of index λ with critical value $c = f(p)$. Suppose that for some $\varepsilon > 0$, the set $f^{-1}([p - \varepsilon, p + \varepsilon])$ contains no critical points of f besides p. Then the space $\mathbb{M}_{c+\epsilon}$ is diffeomorphic to the manifold obtained by attaching a λ-handle to $\mathbb{M}_{c-\epsilon}$. That is, $\mathbb{M}_{c+\epsilon}$ is diffeomorphic to $\mathbb{M}_{c-\epsilon} \cup \mathbb{D}^{\lambda} \times \mathbb{D}^{d-\lambda}$, where $\mathbb{D}^{\lambda}$ denotes a λ-dimensional disk.*

Summarizing, the sublevel sets of a Morse function change precisely when passing through a critical value. Moreover, this change is completely characterized topologically by the index of the critical point.

2.1.3 Gradient Vector Fields

A *vector field* on a manifold is a smooth section of the tangent bundle. Equivalently, it is a smooth function $v : \mathbb{M} \to T\mathbb{M}$, such that $v(x) \in T\mathbb{M}_x$, where $T\mathbb{M}_x$ is the tangent space of $\mathbb{M}$ at x. Given a smooth function $f : \mathbb{M} \to \mathbb{R}$, the *gradient* of f (with respect to the metric $g_{\mathbb{M}}$) is a vector field $\nabla f : \mathbb{M} \to T\mathbb{M}$ consisting of vectors in the direction of the steepest ascent of f, and is formally dual to the differential df. The singularities of ∇f coincide with the critical points of f, and hence are isolated and finite.

2.1.4 Morse–Smale Functions

Let ϕ_t denote the flow generated by ∇f. For a critical point $p \in \mathbb{M}$ of f, the *stable manifold* of p is $S(p) = \{x \in \mathbb{M} \mid \lim_{t \to \infty} \phi_t(x) = p\}$. The *unstable manifold* of p is $U(p) = \{x \in \mathbb{M} \mid \lim_{t \to -\infty} \phi_t(x) = p\}$. A *Morse–Smale function* is a Morse function whose stable and unstable manifolds intersect transversally. The Morse–Smale condition is dependent on the metric $g_{\mathbb{M}}$, but we omit this from the terminology.

An *integral curve* of f passing through a regular point x is $\gamma = \gamma_x : \mathbb{R} \to \mathbb{M}$ defined by $\gamma(t) = \phi_t(x)$. A *flow line* is an equivalence class of integral curves of f, where $\gamma \sim \gamma'$ if $\gamma(t) = \gamma'(s + t)$ for some s and all $t \in \mathbb{R}$. Therefore the unstable and stable manifolds of a critical point are the unions of all flow lines which begin and terminate, respectively, at that critical point. The Morse–Smale condition imposes restrictions on flow lines. For example, flow lines of a Morse–Smale gradient cannot connect critical points of the same index.

For a given Morse–Smale function f, by intersecting the stable and unstable manifolds, we obtain the *Morse–Smale cells* as the connected components of the set $U(p) \cap S(q)$ for all critical points $p, q \in \mathbb{M}$ (Edelsbrunner et al., 2003b). The *Morse–Smale complex* is the collection of Morse–Smale cells (Edelsbrunner et al., 2003b).[1] We define the *Morse–Smale graph* of f to be the 1-skeleton of the Morse–Smale complex, that is, the union of the zero-dimensional (vertices) and one-dimensional (edges) cells of the Morse–Smale complex of f.

---

[1] The Morse–Smale complex described here is treated as a combinatorial structure, not to be confused with Morse–Smale–Witten chain complex (Banyaga and Hurtubise, 2013, Chapter 7).

Remark 1 The Morse–Smale graph is also referred to as the *topological skeleton* in visualization (Helman and Hesselink, 1989), consisting of critical points and streamlines that connect them which divide the domain of ∇f into areas of different flow behavior (referred to as separatrices). A similar invariant is the *distinguished graph* of a gradient-like flow (Peixoto, 1973), allowing for the possibility of maximum-minimum connections, which never occur in the Morse–Smale graph (Edelsbrunner et al., 2003b, Quadrangle Lemma).

Let V_f denote the vertices of the Morse–Smale graph. We define the *decorated Morse–Smale graph* of a Morse function $f\colon \mathbb{M} \to \mathbb{R}$ to be the Morse–Smale graph of f equipped with a vertex weighting given by restricting f to the vertices: $f|_{V_f}\colon V_f \to \mathbb{R}$. Figure 2 is an example of a decorated Morse–Smale graph with the vertex weighting marked next to the critical points. We begin with a Morse function on the sphere $f\colon \mathbb{S}^2 \to \mathbb{M}$ with three maxima, three saddles and two minima. We imagine cutting open and replacing the global minimum with an elastic band, and mapping the sphere to a disk for a clearer visualization.
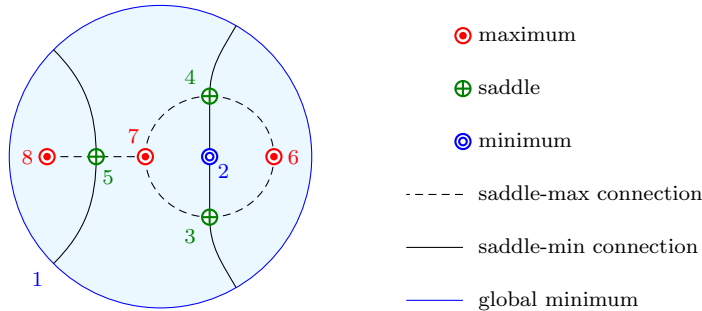

Fig. 2 A decorated Morse–Smale graph for a Morse function on the sphere. The boundary of this disk is identified to a point, which is the global minimum with weight 1.

2.1.5 Filtrations for Persistent Homology

In this paper, we are mostly concerned with *sublevel set* filtrations of functions. That is, we are interested in the topological and algebraic properties of sets $f^{-1}(-\infty, t]$ for $t \in \mathbb{R}$, and inclusion maps among them. Section 4 is an exception, where *level set* and *interlevel set* filtrations are considered, that is, we use sets of the sort $f^{-1}(t)$ and $f^{-1}[t-\epsilon, t+\epsilon]$ for $t \in \mathbb{R}$ and $\epsilon > 0$. We refer the reader to broader surveys such as (Edelsbrunner and Harer, 2010; Bendich et al., 2013) for more on the different ways to approach persistence.

2.2 Equivalences Among Morse Functions

We first review several equivalence relations between Morse functions that have been studied in the literature, including *geometric equivalence*, *topological equivalence*, and *homological equivalence*. We then introduce new notions of equivalence relations between Morse–Smale functions that are essential to our research objectives, namely, *graph equivalence*, *height equivalence*, and *poset equivalence*.

2.2.1 Orientation Preservation and Level Set Preservation

Let $\mathbb{M}$ and $\mathbb{N}$ be smooth, oriented manifolds (of dimension n). A diffeomorphism $h\colon \mathbb{M} \to \mathbb{N}$ is *orientation-preserving* provided that dh_p preserves the orientation at each point p of $\mathbb{M}$, that is, the linear transformation dh_p has positive determinant.

Given two Morse functions on manifolds, $f\colon \mathbb{M} \to \mathbb{R}$ and $g\colon \mathbb{N} \to \mathbb{R}$, a homeomorphism $h\colon \mathbb{M} \to \mathbb{N}$ is *level set preserving* if $h(f^{-1}(a)) = g^{-1}(a)$ for any $a \in \mathbb{R}$. Equivalently, $h\colon \mathbb{M} \to \mathbb{N}$ is level-set preserving if and only if the diagram

$$
\begin{array}{ccc}
\mathbb{M} & \xrightarrow{\quad h \quad} & \mathbb{N} \\
& f \searrow \quad \swarrow g & \\
& \mathbb{R} &
\end{array}
\tag{1}
$$

commutes.

2.2.2 Geometric, Topological and Homological Equivalences

As before, let $f\colon \mathbb{M} \to \mathbb{R}$ be Morse and $\mathbb{M}_t^f := f^{-1}(\infty, t]$ its sublevel sets. For n_f the number of critical points of f, let $a_0 < \cdots < a_{n_f}$ be a sequence of regular values of f such that each interval (a_i, a_{i+1}) contains exactly one critical value of f (for $0 \le i \le n_f - 1$), called a *slicing* (Nicolaescu, 2008) of f. Two Morse functions $f, g\colon \mathbb{M} \to \mathbb{R}$ are *geometrically equivalent* if there exist orientation-preserving diffeomorphisms $r\colon \mathbb{M} \to \mathbb{M}$ and $l\colon \mathbb{R} \to \mathbb{R}$ such that $g = l \circ f \circ r^{-1}$, or equivalently, if the diagram

$$
\begin{array}{ccc}
\mathbb{M} & \xrightarrow{\ r\ } & \mathbb{M} \\
\downarrow{f} & & \downarrow{g} \\
\mathbb{R} & \xrightarrow{\ l\ } & \mathbb{R}
\end{array}
\tag{2}
$$

commutes. The Morse functions f and g are *topologically equivalent* if they have the same number of critical values $n_f = n_g$ and there exists a slicing $a_0 < \cdots < a_{n_f}$ of f and a slicing $b_0 < \cdots < b_{n_g}$ of g together with orientation-preserving diffeomorphisms $\phi_i\colon \mathbb{M}_{a_i}^f \to \mathbb{M}_{b_i}^g$ between sublevel sets. They are *(mod p) homologically equivalent* if they have the same number of critical points and there exists a slicing of f and a slicing of g such that each of the

sublevel sets $\mathbb{M}_{a_i}^f$ and $\mathbb{M}_{b_i}^g$ have the same (mod p) Betti numbers. Note that geometric equivalence implies topological equivalence, which in turn, implies homological equivalence; see (Nicolaescu, 2008) for details.

2.2.3 Graph Equivalence

Two Morse–Smale functions f, g are *graph equivalent* if there is a graph isomorphism $\varphi \colon V_f \to V_g$ with $f|_{V_f} = g|_{V_g} \circ \varphi$. Graph equivalence is strictly stronger than topological equivalence and level-set equivalence, as described in Figure 3.
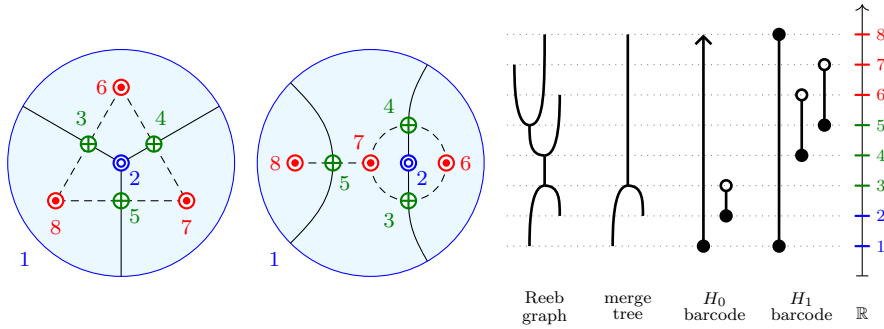

Fig. 3 An example of two Morse functions $\mathbb{S}^2 \to \mathbb{R}$ that have the same barcode, Reeb graph, and merge tree. These functions are geometrically equivalent by (Nicolaescu, 2008, Theorem 3.3), but are not graph equivalent.

2.2.4 Height Equivalence

Let $\iota, \iota' \colon \mathbb{S}^2 \to \mathbb{R}^3$ be smooth embeddings of a sphere to $\mathbb{R}^3$. Let $\pi \colon \mathbb{R}^3 \to \mathbb{R}$ be a projection onto the unit normal vector $[0, 0, 1]^T$. Let $f, g \colon \mathbb{S}^2 \to \mathbb{R}$ be two Morse functions that factor through the two embeddings ι and ι', respectively; that is, $f = \pi \circ \iota$ and $g = \pi \circ \iota'$. Then f and g are called *height equivalent* whenever there is a level set preserving homeomorphism $\psi \colon \mathbb{R}^3 \to \mathbb{R}^3$ with $\iota' = \psi \circ \iota$. Equivalently, f and g are height equivalent if the diagram

$$
\begin{array}{ccc}
 & \mathbb{S}^2 & \\
{\scriptstyle\iota}\swarrow & & \searrow{\scriptstyle\iota'} \\
\mathbb{R}^3 & \xrightarrow{\ \psi\ } & \mathbb{R}^3 \\
{\scriptstyle\pi}\searrow & & \swarrow{\scriptstyle\pi} \\
 & \mathbb{R} &
\end{array}
\tag{3}
$$

commutes. Two height equivalent Morse functions are necessarily equal as functions $\mathbb{S}^2 \to \mathbb{R}$, and thus will have the same critical values and (sub)level set persistence barcodes.

2.2.5 Poset Equivalence

We remind the reader that an *isomorphism* from a poset $(F, \leq_F)$ to a poset $(G, \leq_G)$ is a bijective function $\varphi \colon F \to G$ of sets with the property that, for every x and y in F, $x \leq_F y$ if and only if $\varphi(x) \leq_G \varphi(y)$.

Definition 1 (Poset Equivalence) Two Morse functions $f, g \colon \mathbb{S}^2 \to \mathbb{R}$ factoring through embeddings ι, ι', respectively, are *poset equivalent* if they are height equivalent, and if

1. there exists a common slicing $a_0 < \cdots < a_n$ of f and g such that, for every i, the sets $F_i := \pi_0 \left(\pi^{-1}(a_i) - \iota \circ f^{-1}(a_i) \right)$ and $G_i := \pi_0 \left(\pi^{-1}(a_i) - \iota' \circ g^{-1}(a_i) \right)$ have the structure of a poset, and
2. the map $\pi_0 \circ \psi_i \colon F_i \to G_i$ induced by $\psi_i \colon \left(\pi^{-1}(a_i) - \iota \circ f^{-1}(a_i) \right) \to \left(\pi^{-1}(a_i) - \iota' \circ g^{-1}(a_i) \right)$ is an isomorphism of posets, where ψ_i is a restriction of ψ to the planes $\pi^{-1}(a_i)$.

This equivalence is necessary for understanding the preimage of the persistence map in Section 4. Both Figure 6(a) and Figure 6(c) give two examples of this poset structure, and Figure 7 describes these examples in the context of their Morse functions.

2.2.6 Comparison of Equivalence Relations

We conclude this section with a comparison of the equivalence relations introduced thus far, for Morse functions $f \colon \mathbb{S}^2 \to \mathbb{R}$.

Lemma 1 *The following are strict implications among the equivalence relations.*

$$poset \implies height \implies geometric \implies topological \implies homological$$
$$\Downarrow$$
$$graph$$

Proof In the top line, the first implication follows directly by definition, and is strict by the example of Figure 7. The second implication follows from taking $r = \mathrm{id}_{\mathbb{S}^2}$ and $l = \mathrm{id}_{\mathbb{R}}$ in Diagram (2). Given any Morse function $f \colon \mathbb{S}^2 \to \mathbb{R}$, and sufficiently small ϵ, the functions f and $f + \epsilon$ are geometrically equivalent, but not height equivalent (because they are distinct). The third and fourth implications are shown in (Nicolaescu, 2008), and Figure 5 in the same paper shows that the third implication is strict. As topological equivalence considers orientation while homological equivalence does not, examples abound of why the fourth implication is strict. Figure 3 gives an example of two Morse functions that are geometrically equivalent but not graph equivalent. $\square$

Both the cell decomposition in the decorated Morse–Smale graph and recent work (Martínez-Alfaro et al., 2016, Theorem 1) suggest that graph equivalence implies geometric equivalence. However, this remains an open problem.

Remark 2 If two functions $f, g \colon \mathbb{S}^2 \to \mathbb{R}$ are homologically equivalent, this does not imply they have the same barcode. However, if we instead consider ε-interleavings (Chazal et al., 2009) of barcodes (thought of as persistence modules), then homological equivalence does imply an ε-interleaving.

3 Fundamental Moves

We focus on understanding how cells (generically as quadrangles) of a Morse–Smale complex fit together on a surface and how they change when a pair of critical points is added or removed. We only consider Morse–Smale complexes that arise from a Morse-Smale function on a sphere, and we refer to the changes as fundamental moves, or *moves* in short. Our first main result is to define moves on the Morse–Smale complex, with the goal of describing all the possible ways to create a new Morse–Smale function.

By the Quadrangle Lemma (Edelsbrunner et al., 2003b), every face (cell) of a decorated Morse–Smale graph has four edges, counting an edge twice if the face is on both sides of the edge. This allows us to describe changes to the graph as a composition of moves.

The gradient of a Morse–Smale function gives rise to a Morse–Smale vector field, therefore our approach equivalently describes changes to a Morse–Smale vector field due to the moves, with the changes limited to a particular region of cells for each move. Everything in the vector field outside of this region stays the same between moves. As we only investigate Morse–Smale functions on a manifold, by definition, all saddles are simple; that is, every saddle has degree four, and the endpoints of the four adjacent edges alternate between maxima and minima. All higher-order saddles can be unfolded into simple saddles. As in Figure 2, a saddle-maximum connection is indicated by a solid line, and a saddle-minimum connection is marked by a dashed line. Maxima and minima may have arbitrary degrees.

We now describe face moves, edge moves, and vertex moves; which operate on faces, edges, and vertices, respectively. All of the moves add or remove two cells to the quadrangulation, or equivalently, they add or remove one saddle-maximum or saddle-minimum pair.

Definition 2 (Face Moves) A *face move* is addition (cancellation) of a pair of critical points in the interior of a cell.
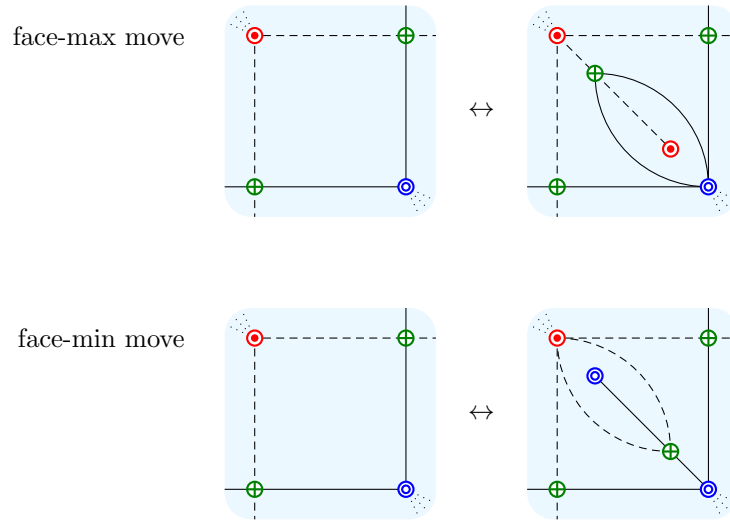
Definition 3 (Edge Moves) An *edge move* is addition (cancellation) of a pair of critical points on the edge of a cell.
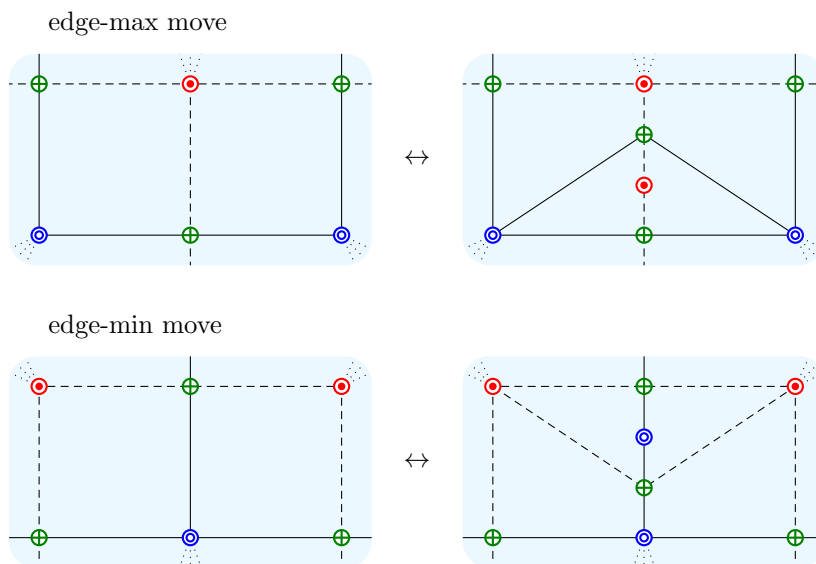
Definition 4 (Vertex Moves) A *vertex move* is addition (cancellation) of
a pair of critical points at an existing critical point.

vertex-max move

vertex-min move
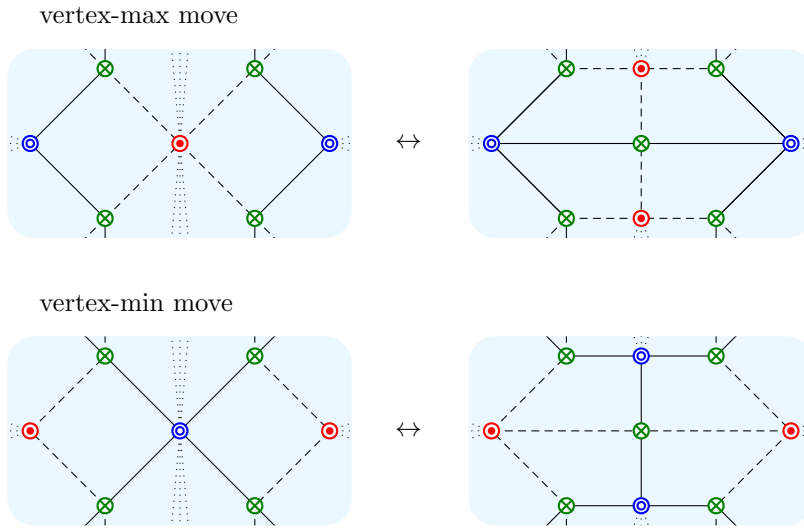
The face, edge, and vertex moves are ways of manipulating the Morse–
Smale complex to obtain another Morse–Smale complex. These moves do not
have functional values associated with the critical points, so they are manip-
ulations of the Morse–Smale complex and not of the underlying function.

Theorem 3 *The Morse–Smale graph of any two Morse–Smale functions is
related by a sequence of face, edge, and vertex moves.*

The proof of this theorem relies on the following restriction imposed on
the Morse–Smale graph. We recall this fact from Edelsbrunner et al. (2003b)
without proof.

Lemma 2 (Quadrangle Lemma) *Each region of the Morse–Smale complex
is a quadrangle with vertices of index 0, 1, 2, and 1, in this order around the
region. The boundary is possibly glued to itself along vertices and arcs.*

Proof (Proof of Theorem 3) We recall the following fact due to Cerf (1970):
any two Morse functions on a manifold $\mathbb{M}$, and therefore any two Morse flows,
can be connected by a path in the space of all smooth functions on $\mathbb{M}$. Further-
more, this path can be chosen to be comprised of Morse functions for all but
finitely many times – at which times the function has a single cubic degener-
ate critical point – in addition to non-degenerate critical points. As one moves
along this path of functions, the cubic degenerate critical point either gives rise
or removes two non-degenerate critical points. Translating this general result
to the Morse–Smale complex of a surface, it suffices to consider introducing
or removing a pair of critical points into a quadrangle decomposition of the

surface. Depending on where we introduce this pair, we shall obtain the different moves of Definitions 2–4. Notice that since the cubic degenerate critical point must give rise to critical points of adjacent index, a saddle point must always be involved in these moves. Since adding and removing critical points are symmetric operations, we only discuss the case of adding critical points.

First suppose the pair of critical points is added in the interior of a quadrangle. Then, as in Figure 4, the introduced saddle must have two flow lines to a single vertex on the boundary of the quadrangle. If a maximum-saddle pair is added, the additional saddle must have two flow lines to the unique minimum, and for an added minimum-saddle pair, the saddle must have two flow lines to the unique maximum. This completely determines the move, and hence is the face-max or face-min move.
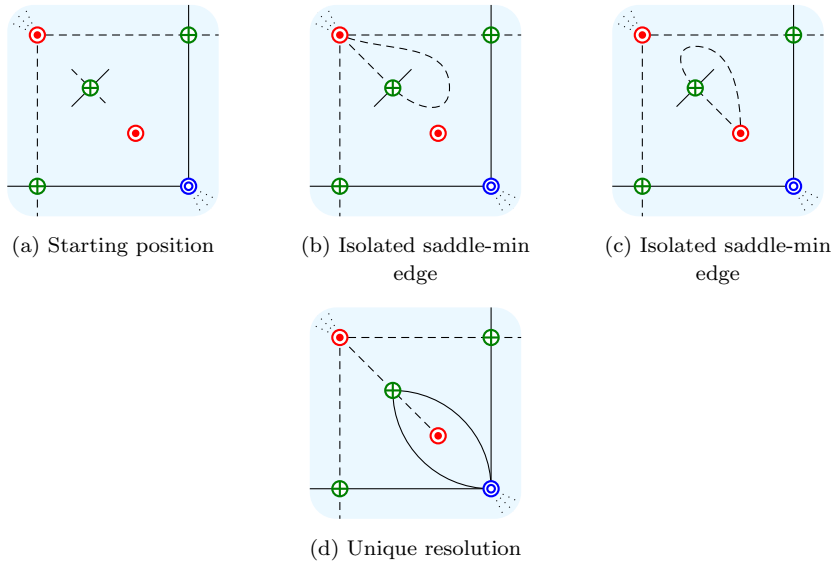

(a) Starting position   (b) Isolated saddle-min edge   (c) Isolated saddle-min edge

(d) Unique resolution

Fig. 4 New edges are uniquely determined when a pair of critical points is added in the interior of a quadrangle.

Next, suppose the pair is added on an edge between two quadrangles. Note that a maximum-saddle pair cannot be added on a separatrix between a minimum and a saddle, and vice-versa, since such a pair would force the saddle in the initial separatrix to have more than four flow lines incident to it. However, adding a maximum-saddle pair to the separatrix between a maximum and a saddle is permissible. In this case, there is a unique way of adding flow lines to obtain a valid configuration, and this is precisely the edge-max move. The edge-min move case is proven similarly.

Finally, suppose the pair is added at a vertex in the quadrangulation. As in the edge moves, a maximum-saddle pair cannot be added at a minimum, and a minimum-saddle pair cannot be added at a maximum. For example, if a

minimum-saddle pair was added at a maximum, a quadrangle would be formed with two minima and two saddles, contradicting the Quadrangle Lemma. Suppose a minimum-saddle pair was added at a minimum. Then, the additional saddle must connect to two maxima. If it connects to the same maximum twice, this is a face move. If it connects to two adjacent maxima, meaning they are both connected to a saddle in the quadrangulation, then this is an edge move. Otherwise, the saddle connects to two maxima, and we have the vertex move. The max-saddle case gives rise to the vertex-max move and is proven similarly.   □

As the fundamental moves add critical points, the moves change the equivalence class (of the classes described in Section 2.2) of the associated Morse–Smale function. However, different moves may give the same change of equivalence class, as witnessed by their Reeb graphs in Figure 5. These changes in the Reeb graph are termed *elementary deformations of B-type* and *D-type* by Di Fabio and Landi (2016), though their analysis emphasizes movement of critical values past each other (see Section 6.3 for further discussion).
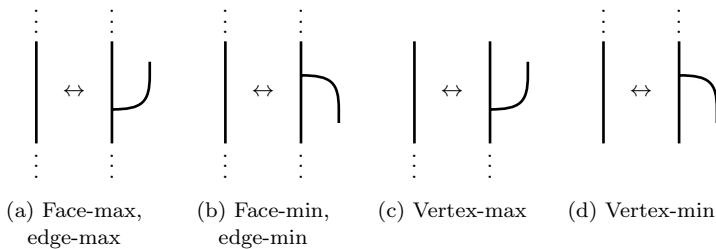

(a) Face-max,   (b) Face-min,   (c) Vertex-max   (d) Vertex-min
    edge-max   edge-min

Fig. 5 Changes to the Reeb graph by the fundamental moves.

Moreover, attempting to consider notions of "distance" on the fundamental moves, as in d'Amico et al. (2010); Bauer et al. (2018), gives no meaningful results, as not specifying critical values allows these distances to be infinitesimally small.

Remark 3 The fundamental moves also have implications for the space of all vector fields, with topology induced by distance between functions. This infinite-dimensional stratified space has strata within which vector fields are Morse–Smale, and the lower-dimensional strata are where transversality of the stable and unstable manifolds fails to hold. Hence the described operations identify different types of lower-dimensional strata, and may be used to count the number of strata within some parameters.

4 The Nesting Poset

To study poset equivalence, we employ the nesting poset introduced in Section 2. The nesting poset is used to study the level sets of a Morse function,

and describe relations among the posets by using the topology of associated level sets. We also show that the nesting poset is a circle containment order, following research in geometric containment orders (Fishburn and Trotter, 1999).

4.1 The Nesting Poset of Level Sets

We first show that the poset isomorphism condition (2) in Definition 1 can be formulated as a nesting poset isomorphism, or equivalently as a circle containment order isomorphism.

4.1.1 Nesting Poset of Jordan Curves

A *Jordan curve* is a non-self-intersecting continuous loop in the plane. Formally, a Jordan curve is a simple closed curve in $\mathbb{R}^2$ that is the image of an injective continuous map $\phi\colon \mathbb{S}^1 \to \mathbb{R}^2$. Let $\gamma := \mathrm{im}(\phi)$ denote a Jordan curve. The Jordan curve theorem (Veblen, 1905) states that the complement $\mathbb{R}^2 - \gamma$ of every Jordan curve γ consists of exactly two connected components: one bounded interior component, denoted as $\mathrm{int}(\gamma)$, and one unbounded exterior component. In this paper, we consider two Jordan curves γ_1 and γ_2 to be *semi-disjoint* if they intersect at a single point ($\gamma_1 \cap \gamma_2 = *$). Two nonidentical Jordan curves are *nested* if $\mathrm{int}(\gamma_1) \subseteq \mathrm{int}(\gamma_2)$ or vice versa.

Given a set of m Jordan curves $\Gamma := \{\gamma_1, \ldots, \gamma_m\}$ with at most one pair of semi-disjoint curves (and the rest are disjoint), its complement $\mathbb{R}^2 - \Gamma$ consists of exactly $m+1$ connected components: m bounded components and one unbounded component.

Remark 4 Let $P := \pi_0(\mathbb{R}^2 - \Gamma)$ denote the set of (path-)connected components of $\mathbb{R}^2 - \Gamma$. The closure of each bounded component in P is a collection of elements of Γ, consisting of an exterior boundary and zero or more interior boundaries. With a slight abuse of notation, we speak of the boundary of a component in P as the boundary of its closure. Let $p_i \in P$ denote the component whose exterior boundary is $\gamma_i \in \Gamma$; let $p_0 \in P$ denote the unbounded component. Let $\partial(p_i)$ denote the set of boundary curves of p_i, where we note that $\partial(p_0)$ contains only interior boundaries. Two components $p_i, p_j \in P$ are *adjacent* if they share a boundary in Γ, that is, $\partial(p_i) \cap \partial(p_j) \in \Gamma$.

Definition 5 (Nesting Poset of Jordan Curves) Let $\Gamma = \{\gamma_1, \ldots, \gamma_n\}$ and $P = \pi_0(\mathbb{R}^2 - \Gamma)$ be as above. For any two adjacent components $p_i, p_j \in P$, define a binary relation $\leq$, such that $p_i \leq p_j$ if and only if (1) $\mathrm{int}(\gamma_i) \subseteq \mathrm{int}(\gamma_j)$, or (2) p_j is unbounded. The *nesting poset* associated to Γ is $N(\Gamma) := (P, \leq_P)$, where $\leq_P$ is the transitive closure of $\leq$ on P.

Reflexivity, anti-symmetry, and transitivity of $\leq_P$ follow from the same properties of set containment $\subseteq$, so $N(\Gamma)$ is indeed a poset. Figure 6 illustrates five examples of Jordan curves (in white) on the plane. Curves in Figure 6(a), Figure 6(b), and Figure 6(d) are disjoint; while curves in Figure 6(c)

and Figure 6(e) are semi-disjoint. For each set Γ, the nesting poset $N(\Gamma)$ is visualized by its Hasse diagram: each vertex corresponds to an element in P (a green shaded region); each arrow indicates a binary relation between adjacent elements (that is, an arrow exists from p_i to p_j if and only if $p_i \leq p_j$).
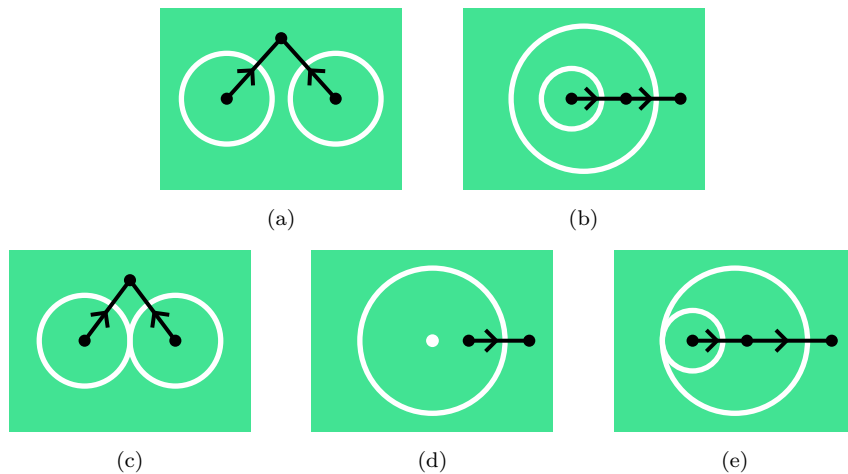

(a)   (b)

(c)   (d)   (e)

Fig. 6 Poset structures of level sets of some Morse functions for two regular values (a, b), and three critical values, (c, d, and e).
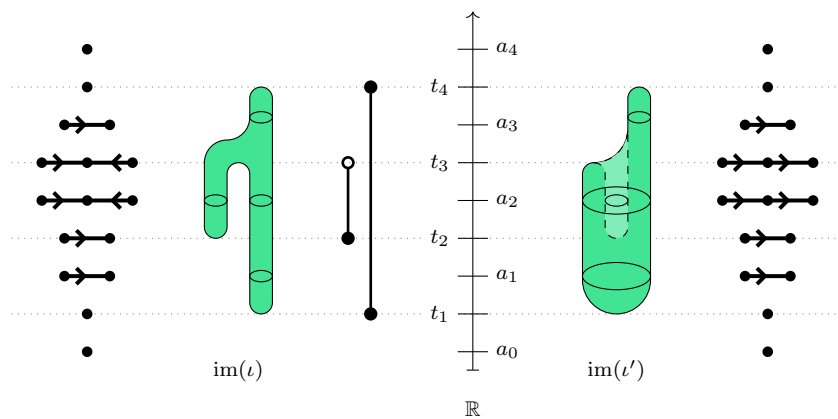

Fig. 7 A Morse function factoring through two different embeddings ι, ι', which are height equivalent but not poset equivalent, as distinguished by their different nesting posets.

4.1.2 Nesting Poset of Level Sets

Let $f\colon \mathbb{S}^2 \to \mathbb{R}$ be a Morse function that factors through a smooth embedding ι; that is, f is defined as the composition $f = \pi \circ \iota$, for $\mathbb{S}^2 \xrightarrow{\iota} \mathbb{R}^3 \xrightarrow{\pi} \mathbb{R}$. Assuming $\mathbb{M}$ is smooth and compact, the level set $f^{-1}(a)$ is a (not necessarily connected) 1-manifold without boundary for a regular value $a \in \mathbb{R}$ according to the Implicit Function Theorem. The set $\iota \circ f^{-1}(a)$ is therefore a set of disjoint Jordan curves in the plane $\pi^{-1}(a) \subset \mathbb{R}^3$. For $a = c$ a critical value of f, the set $\iota \circ f^{-1}(a)$ contains either exactly one pair of semi-disjoint Jordan curves or a point (together with other disjoint Jordan curves).

Definition 6 (Nesting Poset of Level Sets) For any $a \in \mathbb{R}$, let $\Gamma = \iota \circ f^{-1}(a)$ and $P = \pi_0(\pi^{-1}(a) - \Gamma)$. The *nesting poset* N_a associated with a is the nesting poset of Jordan curves Γ in the plane $\pi^{-1}(a)$. With an abuse of notation, $N_a := N(\Gamma) = (P, \leq_P)$.

For example, Figure 6(a) and Figure 6(b) illustrate two sets of disjoint Jordan curves (in white) that arise from level sets of two Morse functions f and g at a shared regular value, respectively. Figure 7 describes these examples in the context of their corresponding Morse functions. Specifically, two Morse functions $f, g\colon \mathbb{S}^2 \to \mathbb{R}$ factor through embeddings $\iota, \iota'\colon \mathbb{S}^2 \to \mathbb{R}^3$ with the same barcode, $f = \pi \circ \iota$ and $g = \pi \circ \iota'$ in Figure 7. For *any* common slicing $a_0 < a_1 < a_2 < a_3 < a_4$, let $F_i := \pi_0\left(\pi^{-1}(a_i) - \iota \circ f^{-1}(a_i)\right)$ and $G_i := \pi_0\left(\pi^{-1}(a_i) - \iota' \circ g^{-1}(a_i)\right)$; the map $F_i \to G_i$ is not a poset isomorphism for $i = 2$; in particular, regular value a_2 gives rise to a poset structure in Figure 6(a) for f and a different one in Figure 6(b) for g. By Definition 1, f and g are not poset equivalent.

4.1.3 Circle Containment Order

A partially ordered set $(P, \leq)$ is called a *circle containment order* (Scheinerman and Wierman, 1988), provided one can assign to each $p_i \in P$ a closed disc in the plane $o_i \subseteq \mathbb{R}^2$ satisfying $p_i \leq p_j$ if and only if $o_i \subseteq o_j$. Let $\alpha\colon P \to \mathbb{R}^2$ denote such an assignment. If $\phi\colon \mathbb{R}^2 \to \mathbb{R}^2$ is an orientation-preserving homeomorphism, then ϕ does not change the circle containment order, so that α and $\phi \circ \alpha$ are equivalent circle containment orders.

The nesting poset structure of $P = \pi_0\left(\pi^{-1}(a) - \iota \circ f^{-1}(a)\right)$, for any regular value a, could be understood in terms of a circle containment order. As illustrated in Figure 6(a), each bounded element in a poset (a green shaded region) $p_i \in P$ (where $i > 0$) can be assigned a closed disc in the plane, which is the bounded interior component $\mathrm{int}(\gamma_i)$. The unbounded component $p_0 \in P$ is assigned a closed disc that enclose all other discs. Such an assignment imposes a circle containment order. Hence a nesting poset is a circle containment order.

4.2 A Morse-Theoretic Perspective on Nesting Posets

Now we provide theorems analogous to Theorems 1 and 2. As before, the Morse function $f\colon \mathbb{S}^2 \to \mathbb{R}$ factors through an embedding ι as $f = \pi \circ \iota$. Let $L_t := \iota \circ f^{-1}(t)$ denote the embedding of its level sets. There are three types of critical points in $\mathrm{im}(\iota)$: local minima, saddles, and local maxima, with indices 0, 1, and 2, respectively. To study local structure surrounding the critical points, we further classify the saddles into *merging saddles* and *splitting saddles* by investigating the relation between level sets $L_{c-\epsilon}$ and $L_{c+\epsilon}$ as t crosses the critical value $c = f(p)$ of a saddle p. If $\epsilon > 0$ is small enough, the intervals $[c - \epsilon, c)$ and $(c, c + \epsilon]$ contain no critical values.

A saddle p is a *merging saddle* if a pair of disjoint Jordan curves in $L_{c-\epsilon}$ merges into a single Jordan curve in $L_{c+\epsilon}$ as t crosses c. A saddle p is a *splitting saddle* if a Jordan curve at $L_{c-\epsilon}$ splits into a pair of disjoint Jordan curves at $L_{c+\epsilon}$ as t crosses c. A merging saddle is of *nesting* type if the Jordan curves that merge at $L_{c+\epsilon}$ are nested at $L_{c-\epsilon}$; otherwise, the saddle is of *non-nesting* type. Similarly, we can define splitting saddles of nesting and non-nesting types. Figures 8 - 12 illustrate the reasoning behind this terminology.
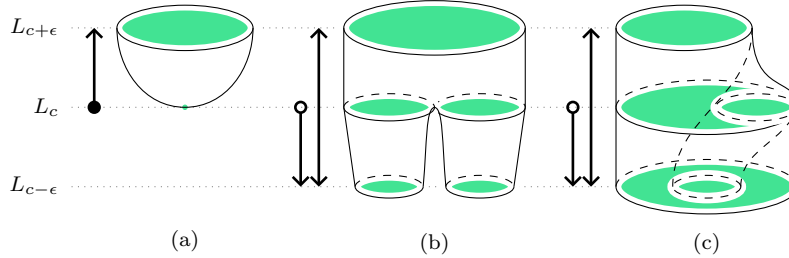

Fig. 8 A local minimum (a), a non-nesting (b) and a nesting (c) merging saddle with their corresponding (partial) zero-dimensional interlevel persistence barcodes.

As before, let $\Gamma = L_t = \iota \circ f^{-1}(t)$ and $N_t = N(\Gamma) = (P, \leq_P)$ be the nesting poset. We now study how N_t changes as $t \in \mathbb{R}$ changes.

Theorem 4 *If f has no critical values in the interval $[a, b]$, then N_a and N_b are poset isomorphic, that is, $N_a \cong N_b$.*

Proof This follows from a key observation in proving Theorem 1 from Morse theory. Recall (Matsumoto, 1997, Theorem 2.31), that if f has no critical values in the interval $[a, b]$, then $\mathbb{M}_{[a,b]} := \{x \in \mathbb{M} \mid a \leq f(a) \leq b\}$ is diffeomorphic to the product $f^{-1}(a) \times [a, b]$. Using the gradient-like vector field for f, the proof of Theorem 2.31 in (Matsumoto, 1997) includes a construction of an orientation-preserving diffeomorphism $h\colon f^{-1}(a) \times [0, b - a] \to \mathbb{M}_{[a,b]}$. Therefore, $\mathbb{M}_{[a,b]}$ is diffeomorphic to $f^{-1}(a) \times [0, b-a]$ and thus also to $f^{-1}(a) \times [a, b]$.

However, we do not study f directly, we instead study the function π restricted to $\mathrm{im}(\iota)$ and sublevel sets $L_{[a,b]} := \iota \circ f^{-1}[a, b]$. Nonetheless, Theorem

2.31 from (Matsumoto, 1997) still applies, that is, there exists a diffeomorphism $h\colon L_a \times [0, b-a] \to L_{[a,b]}$ implying $L_{[a,b]} \cong L_a \times [0, b-a]$. The diffeomorphism h is orientation-preserving, therefore it does not change the circle containment order moving from N_a to N_b. Therefore $N_a \cong N_b$. □

Denote an injective map of posets by $\hookrightarrow$ and a surjective map of posets by $\twoheadrightarrow$. If the injective map happens to be an isomorphism, we write $\overset{\cong}{\hookrightarrow}$. The conditions on $f\colon \mathbb{S}^2 \to \mathbb{R}$ are as above.

Theorem 5 *Let p be a critical point of f with critical value $c := f(p)$. Then for ϵ small enough, there exist zigzags of poset maps:*

1. *$N_{c-\epsilon} \overset{\cong}{\hookleftarrow} N_c \hookrightarrow N_{c+\epsilon}$ if p is a local minimum;*
2. *$N_{c-\epsilon} \hookleftarrow N_c \overset{\cong}{\hookrightarrow} N_{c+\epsilon}$ if p is a local maximum;*
3. *$N_{c-\epsilon} \overset{\cong}{\hookleftarrow} N_c \twoheadrightarrow N_{c+\epsilon}$ if p is a non-nesting merging saddle;*
4. *$N_{c-\epsilon} \twoheadleftarrow N_c \overset{\cong}{\hookrightarrow} N_{c+\epsilon}$ if p is a non-nesting splitting saddle;*
5. *$N_{c-\epsilon} \overset{\cong}{\hookleftarrow} N_c \hookleftarrow N_{c+\epsilon}$ if p is a nesting merging saddle;*
6. *$N_{c-\epsilon} \hookrightarrow N_c \overset{\cong}{\hookrightarrow} N_{c+\epsilon}$ if p is a nesting splitting saddle.*

As the behavior of nesting posets for local maxima and nesting/non-nesting splitting saddles of f is the same as local minima and nesting/non-nesting merging saddles, respectively, of the Morse function $-f$, we only prove Statements 1, 3, and 5 in Theorem 5.

Proof By the Morse Lemma, there exists a neighborhood V of p such that on V, $f(x) = f(p) \pm x_1^2 \pm x_2^2$. The function f is excellent, so there exists some $\epsilon > 0$ such that $f^{-1}[c - \epsilon, c + \epsilon]$ contains only one critical point of f, namely p. Let $U := f^{-1}[c - \epsilon, c + \epsilon] \cap V$. Then ∇f provides a diffeomorphism from $f^{-1}(c-\epsilon) \setminus U$ to $f^{-1}(c+\epsilon) \setminus U$. By Theorem 4, the nesting poset is unchanged outside of U, hence the proof is reduced to a local computation of the nesting poset of U for each case.

For every $t \in [c-\epsilon, c+\epsilon]$, let $L_t := \iota(f^{-1}(t) \cap V)$ and let $L := \bigcup_{t \in [c-\epsilon, c+\epsilon]} L_t$. Take a contractible neighborhood W of L, and without loss of generality assume that $L \subseteq \pi^{-1}[c - \epsilon, c + \epsilon]$ and $W_t := \pi^{-1}(t) \cap W$ is non-empty and contractible for every $t \in [c - \epsilon, c + \epsilon]$. Note that $\iota \circ f^{-1}[c - \epsilon, c + \epsilon]$ may contain more than one connected component. This proof proceeds functorially, by describing for every $t \leqslant s \in [c - \epsilon, c + \epsilon]$ a map of posets $N_t \to N_s$ induced by the topological inclusions $W_t - L_t \hookrightarrow (W - L) \cap \pi^{-1}[t, s]$ and $W_s - L_s \hookrightarrow (W - L) \cap \pi^{-1}[t, s]$.

For Statement 1, the function f has index 0 and so $f(x) = f(p) + x_1^2 + x_2^2$ in V. As in Figure 9, assign labels to the connected components of the three (subsets of) level sets $W_{c-\epsilon} \subseteq \pi^{-1}(c-\epsilon)$, $W_c - L_c \subseteq \pi^{-1}(c)$, and $W_{c+\epsilon} - L_{c+\epsilon} \subseteq \pi^{-1}(c + \epsilon)$. The topological inclusion $A' \hookrightarrow A$ and the natural injective map $A' \hookrightarrow A''$ that widens the hole of A' induce analogous maps on the nesting posets $N_c \to N_{c-\epsilon}$ and $N_c \to N_{c+\epsilon}$, respectively. The poset elements are given
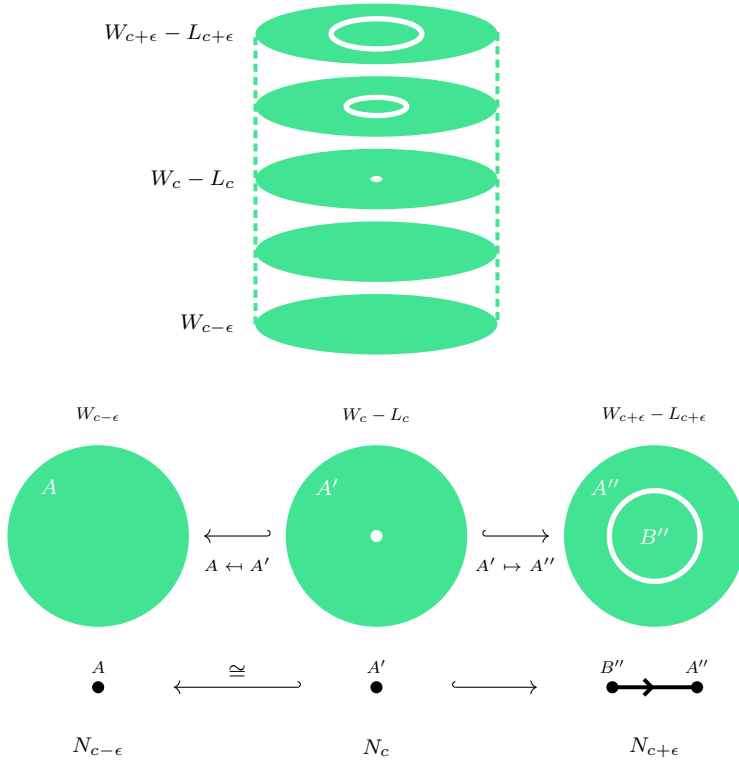
Fig. 9 Topological construction and labelling for Statement 1.

the same labels as the connected components to which they correspond, and their relation is defined in Definition 6.

For Statements 3 and 5, the function f has index 1 and so $f(x) = f(p) - x_1^2 + x_2^2$ up to diffeomorphism. As in Figure 10, assigning labels coherently to the connected components of the three (subsets of) level sets is ambiguous, as some may connect beyond W. It is necessary to clarify this, as we want an injective map from the nesting poset constructed from $W_t - L_t$ to the nesting poset constructed from $\pi^{-1}(t) - \iota(f^{-1}(t))$.

To resolve this, take a larger neighborhood $W' \supseteq W$ so that $W'_t := W' \cap \pi^{-1}(t)$ contains some connected components of the embedded 1-manifold $\iota(f^{-1}(t))$, for every $t \in [c - \epsilon, c + \epsilon]$ a regular value (and contains an embedded $\mathbb{S}^1 \vee \mathbb{S}^1$ for t a critical value). There are 4 unique embeddings, up to diffeomorphism, as shown in Figure 13, among which Figure 13(a) corresponds to Statement 3 and Figure 13(c) corresponds to Statement 5.

For Statement 3, as in Figure 11, assign labels to the connected components of the (subsets of) level sets $W'_{c-\epsilon} - \iota(f^{-1}(c-\epsilon))$, $W'_c - \iota(f^{-1}(c))$, and $W'_{c+\epsilon} - \iota(f^{-1}(c+\epsilon))$. The topological inclusions $A' \hookrightarrow A$, $B' \overset{\cong}{\hookrightarrow} B$, and $C' \overset{\cong}{\hookrightarrow} C$ induce an analogous nesting poset $N_c \to N_{c-\epsilon}$. Similarly, the topological surjections
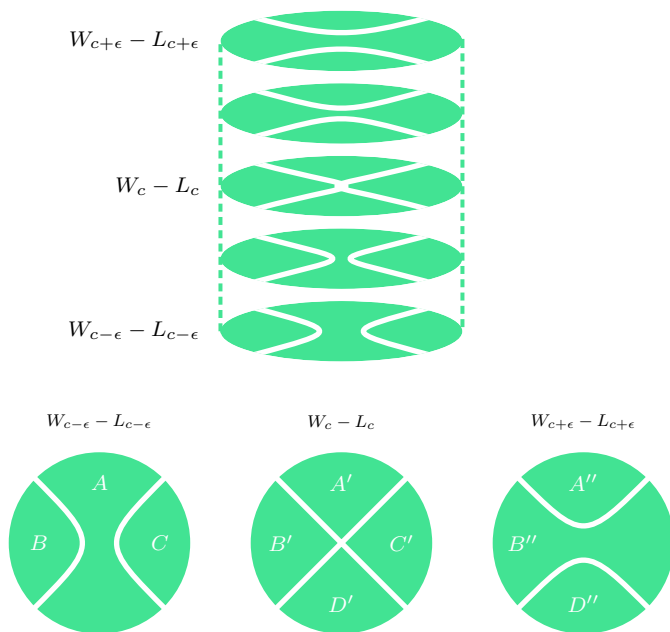
Fig. 10 Ambiguity in coherent component labeling of (subsets of) level sets near a saddle.

$A' \xrightarrow{\cong} A''$, $B' \xrightarrow{\cong} B''$, and $C' \xrightarrow{\cong} B''$ induce an analogous nesting poset map $N_c \to N_{c+\epsilon}$.
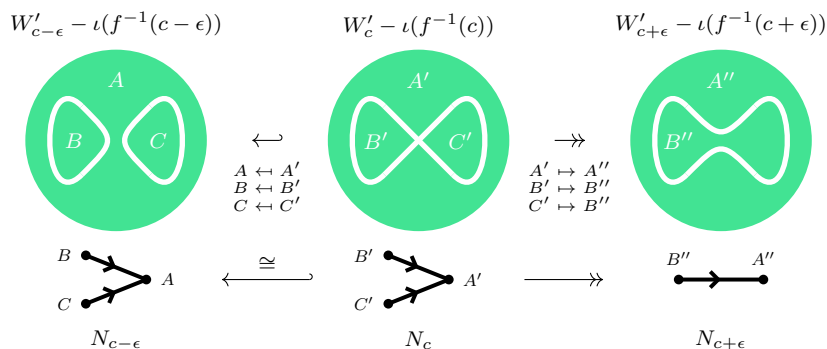

Fig. 11 Topological construction and labelling for Statement 3.

For Statement 5, as in Figure 12, assign labels to the connected components of the (subsets of) level sets $W'_{c-\epsilon} - \iota(f^{-1}(c-\epsilon))$, $W'_c - \iota(f^{-1}(c))$, and $W'_{c+\epsilon} - \iota(f^{-1}(c+\epsilon))$. The topological inclusions $A' \hookrightarrow A$, $B' \overset{\cong}{\hookrightarrow} B$, and $C' \overset{\cong}{\hookrightarrow} C$ induce an analogous nesting poset $N_c \to N_{c-\epsilon}$. Similarly, the topological inclusions
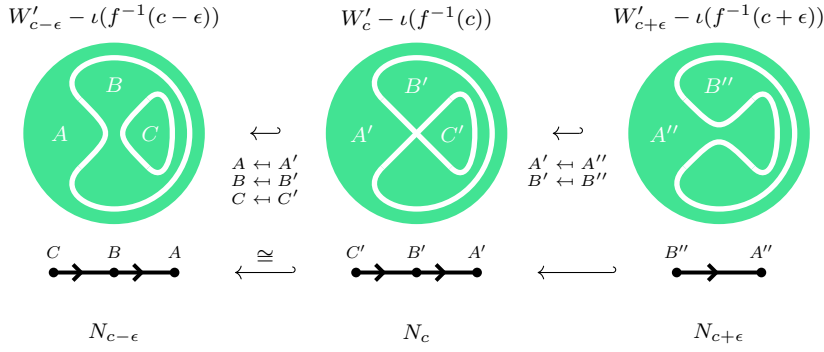
$$W'_{c-\epsilon} - \iota(f^{-1}(c-\epsilon)) \qquad W'_c - \iota(f^{-1}(c)) \qquad W'_{c+\epsilon} - \iota(f^{-1}(c+\epsilon))$$

Fig. 12 Topological construction and labelling for Statement 5.

$A'' \overset{\cong}{\hookrightarrow} A'$ and $B'' \overset{\cong}{\hookrightarrow} B'$ induce an analogous nesting poset map $N_{c+\epsilon} \to N_c$. □

Note that the maps in Statements 1 - 4 all have a zigzag structure $N_{c-\epsilon} \leftarrow N_c \to N_{c+\epsilon}$, but Statements 5 and 6 do not. One may enforce such maps on Statements 5 and 6, and following Figure 12 we have two choices. One choice is to map C' and A' both to A'', following the induced topology, but that would collapse the poset down to a single point, as we require order-preservation. The second choice is to map C' and B' both to B'', but that would break functoriality and not follow the topology of the neighborhood.

Remark 5 We mention some observations from this section so far.

1. The nesting poset doesn't see the critical value in $[c - \epsilon, c]$ if c is merging or a minimum, because the interiors have not merged yet.
2. Functoriality seems to hold from the category of topological spaces **Top** to the category of posets and order-preserving maps. However, we only assigned poset maps to particular topological inclusions, not all of them, as mentioned in the comment after the proof of Theorem 5, so functoriality may hold for an appropriately defined subcategory of **Top**.
3. In Figures 9, 11, 12 there was always a largest poset element, and in fact N_t always has a maximal element representing the unbounded component of $\pi^{-1}(t) - \iota(f^{-1}(t))$. The poset maps always send the maximal element to the maximal element, so it does not contain any interesting information.

For completeness, we include in Figure 13 an exhaustive description, up to diffeomorphism, of all of the choices presented by the ambiguous connected component labelling from Figure 10.
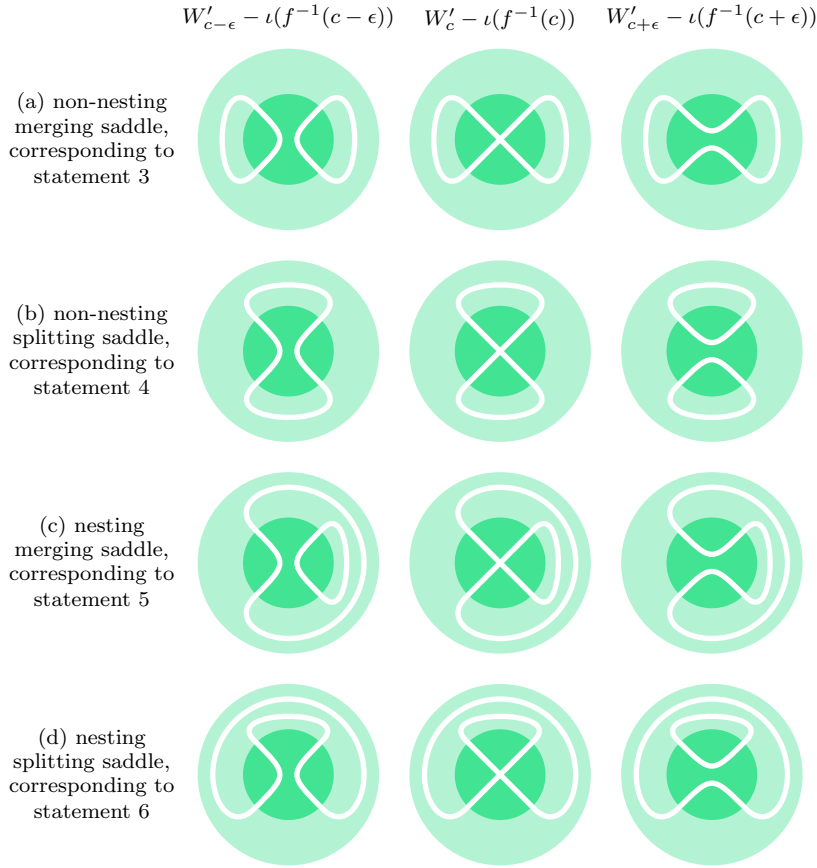
$$W'_{c-\epsilon} - \iota(f^{-1}(c-\epsilon)) \qquad W'_c - \iota(f^{-1}(c)) \qquad W'_{c+\epsilon} - \iota(f^{-1}(c+\epsilon))$$

(a) non-nesting merging saddle, corresponding to statement 3

(b) non-nesting splitting saddle, corresponding to statement 4

(c) nesting merging saddle, corresponding to statement 5

(d) nesting splitting saddle, corresponding to statement 6

Fig. 13 Larger neighborhoods $W' \supseteq W$ corresponding to Statements 3-6 of Theorem 5.

4.3 The Zigzag of Posets

4.3.1 Combinatorial Barcode

We now have a zigzag structure along $\mathbb{R}$ of the nesting posets of f. This new data will allow us to augment the data of the barcode with a new type of barcode that combinatorially describes a Morse function factoring through an embedding by a height projection.

Corollary 1 *Given a slicing $a_0 < t_1 < a_1 < \cdots < t_n < a_n$, there is a zigzag of posets*

$$N_{a_0} \xleftrightarrow{\varphi_0^-} N_{t_1} \xleftrightarrow{\varphi_0^+} N_{a_1} \xleftrightarrow{\varphi_1^-} N_{t_2} \xleftrightarrow{\varphi_1^+} \cdots \xleftrightarrow{\varphi_n^-} N_{t_n} \xleftrightarrow{\varphi_n^+} N_{a_n}, \tag{4}$$

where the direction of each $\varphi_i^\pm$ is defined by Theorem 5.

This follows directly from Theorem 5. Note that every backwards map φ in the zigzag (4) can be reversed using the Galois connection construction (Roman, 2008, Chapter 3) with

$$\varphi^{\dagger}(y) := \max\{x : \varphi(x) \leq y\}, \tag{5}$$

though we are only guaranteed $\varphi^{\dagger}(\varphi(x)) \geq x$. That is, while we do get a diagram

$$N_{a_0} \longrightarrow N_{t_1} \longrightarrow N_{a_1} \longrightarrow \cdots \longrightarrow N_{t_n} \longrightarrow N_{a_n} \tag{6}$$

of posets, it does not capture splitting saddles (neither nesting nor non-nesting). Hence we instead explore a combinatorial barcode with $\mathbf{k}$-algebras corresponding to posets in a persistence module.

Remark 6 The zigzag (4) is reminiscent of diagrams in zigzag persistence (Carlsson and de Silva, 2010), and at first glance it seems possible to recover (4) by taking the nesting posets of spaces whose homology is taken to compute zigzag persistence. However, in zigzag persistence the considered spaces are of the sort $f^{-1}[t, s]$, whereas in our case we compute the nesting poset of (a subset of) $f^{-1}(t)$. For such t, there does not always exist $\epsilon > 0$ such that $f^{-1}(t \pm \epsilon)$ is the same nesting poset as for $f^{-1}(t)$, and so computing the nesting poset of an interlevel set does not make sense in our context. Nonetheless, there are modifications (Kim and Memoli, 2018) of this approach that hold promise for applications.

For a poset P, an *interval* I in P is a connected subposet $I \subseteq P$ such that for any $x, y \in I$, $x \leq t \leq y$ implies $t \in I$. When the poset if finite, an interval I is generated by two endpoints, and we write $I = [a, b] := \{t \in P : a \leq t \leq b\}$. The following definition comes from Charalambides (2019).

Definition 7 The *incidence algebra* $\mathbf{k}P$ of a poset P is the free vector space over $\mathbf{k}$ generated by set of intervals I of P. Multiplication $\times : \mathbf{k}P \times \mathbf{k}P \to \mathbf{k}P$ is given by concatenation of compatible intervals

$$[c, d] \times [a, b] = \begin{cases} [a, d] & \text{if } b = c \\ 0 & \text{else,} \end{cases}$$

and multiplication is 0 for unconcatenable intervals, making $\mathbf{k}P$ a $\mathbf{k}$-algebra.

Conjecture 1 There is a zigzag module of $\mathbf{k}$-algebras

$$\mathbf{k}N_{a_0} \leftrightarrow \mathbf{k}N_{t_1} \leftrightarrow \mathbf{k}N_{a_1} \leftrightarrow \mathbf{k}N_{t_2} \leftrightarrow \cdots \leftrightarrow \mathbf{k}N_{t_n} \leftrightarrow \mathbf{k}N_{a_n},$$

with arrow direction given by Corollary 1, that decomposes into a sum of interval indecomposables of the form

$$\mathbf{k}_I(t) = \begin{cases} \mathbf{k}\{*\} & \text{if } t \in I \\ 0 & \text{if } t \notin I. \end{cases}$$

Furthermore, this collection of interval indecomposables determines f up to poset equivalence.

This approach follows the vein of foundational persistent homology results (Crawley-Boevey, 2015; Botnan, 2017) about decomposition of barcodes into fundamental parts. We call this collection of interval indecomposables the *combinatorial barcode* of f.

5 Counting Morse Functions

The observations of the previous section, specifically Figure 8, hint to a method of counting Morse functions by their barcode. In this section, instead of analyzing the local behavior around critical values as before, we start with a global picture of a complete barcode, and use Figure 14 as motivation. As before, $f \colon \mathbb{S}^2 \to \mathbb{R}$ factors as $\pi \circ \iota$, for $\iota \colon \mathbb{S}^2 \to \mathbb{R}^3$ a smooth embedding.
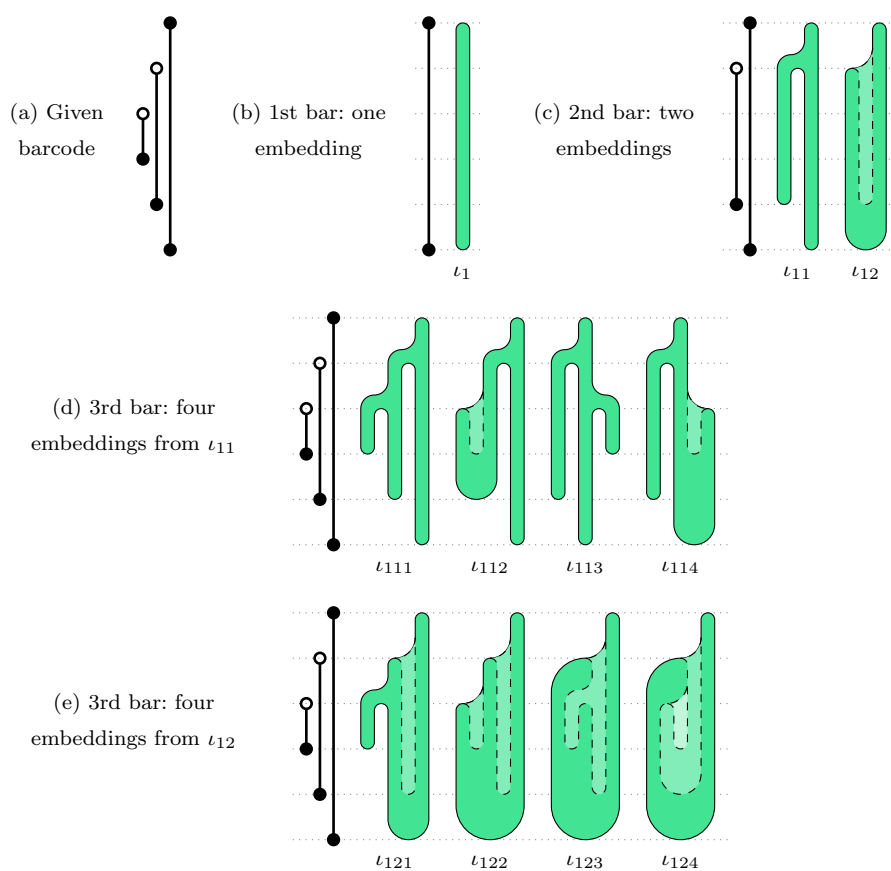

Fig. 14 A motivating example.

Example 1 Suppose f has 6 critical values and a known zero-dimensional barcode consisting of 3 bars nested inside each other, as in Figure 14(a). Construct all embeddings ι of f by considering the effect of each bar on the embedding separately, following the nesting/non-nesting poset approach of Section 4. Begin with the largest bar of the barcode, then add bars in their nesting order. The second bar gives 2 nesting choices. Each of the 2 nesting choices gives 4 more nesting choices, when the smallest bar of the barcode is added.

Example 1 leads immediately to several observations. First note that the types of critical points associated with closed endpoints of barcodes are decided (local minimum at the highest points, local maximum at the lowest points). Second, we see that simply choosing nesting or non-nesting-type at the open barcode endpoints does not give all the embeddings. For example, ι_{111} and ι_{113} have identical critical value types in the same order. Finally, note that the relation between the number of bars and number of embeddings depends upon containment relations among the bars. That is, by considering bars largest to smallest, for every bar contained in a larger one, the number of embeddings computed up to that point doubles. This is more precisely described by Conjecture 2.

Let B be the barcode of f, viewed as a set of subintervals $I_1, \ldots, I_N$ of $\mathbb{R}$. For every $j = 1, \ldots, N$, let $\mu_B(I_j)$ be the number of bars I_k in B such that $I_j \subsetneq I_k$.

Conjecture 2 The number of ways the Morse function f factors through $\mathbb{R}^3$, up to height-equivalence, is bounded below by

$$2^{N-1} \prod_{j=2}^{N} \mu_B(I_j). \tag{7}$$

We leave this conjecture open for future work, and make two observations about why Example 1 is not a generic example.

- The barcode in the example has a single interval whose highest endpoint is closed. Given more than one such interval, the count given in Conjecture 2 would miss such embeddings.
- The barcode in the example does not give rise to embeddings whose branches might be "twisted" in a non-trivial manner. That is, given a barcode with more bars, the count from Conjecture 2 would miss the embeddings with "twists".

6 Discussions

We have characterized the moduli space of classes of Morse functions on the sphere under both functional and dynamic settings. Using persistence as a constraint, we have defined equivalence relations between Morse functions and have studied the combinatorial structure of Morse functions on a sphere modulo such relations. Our approach describes structures in detail, and therefore provides a fruitful ground for continued research in several directions.

6.1 Realizing Preimages of a Barcode

Conjecture 2 considers a counting argument that is only at the beginning of addressing Objective 3 from Section 1. This is given in the context of finding a representative of the preimage of the persistence map

$$\{\text{Morse functions on } \mathbb{S}^2\} \to \{\text{Barcodes}\}, \tag{8}$$

where a barcode is viewed as a multiset of intervals of $\mathbb{R}$. To further answer Objective 3, we may ask: given a barcode B, find an embedding $\iota \colon \mathbb{S}^2 \to \mathbb{R}^3$ such that B is the barcode of $f := \pi \circ \iota$ under level set persistence in degree zero. Note that some barcodes cannot be realized as height-embedded Morse functions on $\mathbb{S}^2$, for example $B = \{[0,3], (1,2)\}$, as any open interval or a closed interval nested in another closed interval is forbidden for the sphere. However, if B has a single closed bar inside which all other bars are contained, we can easily construct a Reeb graph $\mathcal{R}_B$, which in turn may be associated to a diagram of 1-spheres and wedges of 1-spheres, which may then be assembled into an embedding of a 2-sphere, as in Figure 15.
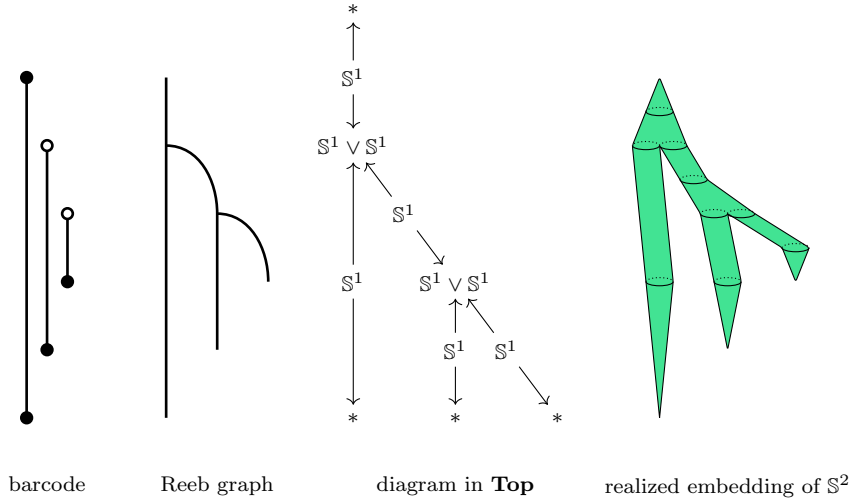

barcode   Reeb graph   diagram in **Top**   realized embedding of $\mathbb{S}^2$

Fig. 15 Constructing a 2-sphere embedding from a barcode.

This construction suggests an algorithmic approach to constructing embeddings $\iota \colon \mathbb{S}^2 \to \mathbb{R}^3$ such that the barcode of the height function on $\mathrm{im}(\iota)$ will produce the barcode B. That is, every vertex of the Reeb graph of degree $n \geqslant 3$ corresponds to a wedge of $n-1$ spheres, every vertex of degree 1 corresponds to a point, and every edge between vertices corresponds to a zigzag $X \leftarrow \mathbb{S}^1 \to Y$ in **Top**. We leave the formalization and extension of these ideas open for further research.

6.2 Extending the Nesting Poset

Theorem 5 and its proof used arguments based on including smaller topological spaces into larger ones. Using the critical values of f, every open interval of $\mathbb{R}$ containing at most one critical value can be uniquely associated with a nesting poset. Then the maps described in Theorem 5 correspond to restriction to a subset or containment in a superset, the former case described in Figure 16, following Figure 11.
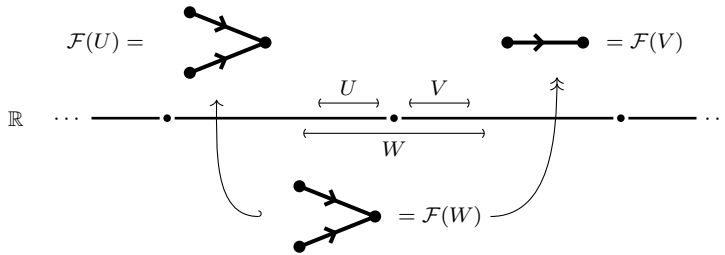

Fig. 16 Associating poset maps to set restrictions.

What we have described suggests the structure of an $\mathbb{R}$-*constructible sheaf* encoding the nesting poset. More detail is given by Curry and Patel (2016) as well as by MacPherson and Patel (2018) but we do not explore this here and leave it open for further research.

6.3 Keeping Track of Critical Values

The techniques we have described here are concerned with the relative order of critical values, and only as a consequence of other structural changes. Using the order of critical values as a primary motivator opens up new directions of research, some of which are addressed by ongoing work in vector field design (Zhou et al., 2019) and existing literature on distances for topological invariants Di Fabio and Landi (2016); Bauer et al. (2018); d'Amico et al. (2010).

In addition, specifying function values on singularities would allow for an additional measure on how "far apart" two functions are: one could use the number of moves together with the difference of function values to measure their differences. The "complexity" of a Morse function f could then be given by measuring the difference between f and a baseline function, such as the height function h on the standard embedding of $\mathbb{S}^2$ in $\mathbb{R}^3$.

Conflict of interest

The authors declare that they have no conflict of interest.

References

H. Adams and G. Carlsson. Evasion paths in mobile sensor networks. *International Journal of Robotics Research*, 34(1):90–104, 2015.

V. I. Arnold. Bernoulli-Euler updown numbers associated with function singularities, their combinatorics and arithmetics. *Duke Mathematical Journal*, 63(2):537–555, 1991.

V. I. Arnold. The calculus of snakes and the combinatorics of Bernoulli, Euler and Springer numbers of Coxeter groups. *Russian Mathematical Surveys*, 47(1):1, 1992.

V. I. Arnold. Topological classification of Morse functions and generalisations of Hilbert's 16-th problem. *Mathematical Physics, Analysis and Geometry*, 10(3):227–236, 2007.

A. Banyaga and D. Hurtubise. *Lectures on Morse Homology*, volume 29. Springer Science & Business Media, 2013.

U. Bauer and M. Lesnick. Induced matchings and the algebraic stability of persistence barcodes. *Journal of Computational Geometry*, 6(2):162–191, 2015.

U. Bauer, C. Landi, and F. Memoli. The Reeb graph edit distance is universal. arXiv:1801.01866, Jan. 2018.

P. Bendich, H. Edelsbrunner, D. Morozov, and A. Patel. Homology and robustness of level and interlevel sets. *Homology, Homotopy and Applications*, 15:51–72, 2013.

S. Biasotti, L. De Floriani, B. Falcidieno, P. Frosini, D. Giorgi, C. Landi, L. Papaleo, and M. Spagnuolo. Describing shapes by geometrical-topological properties of real functions. *ACM Computing Surveys (CSUR)*, 40(4):1–87, 2008.

M. B. Botnan. Interval decomposition of infinite zigzag persistence modules. *Proceedings of the American Mathematical Society*, 145(8):3571–3577, 2017.

P. Bubenik, M. Hull, D. Patel, and B. Whittle. Persistent homology detects curvature. *Inverse Problems*, 36(2), Jan. 2020.

G. Carlsson and V. de Silva. Zigzag persistence. *Foundations of Computational Mathematics*, 10(4):367–405, 2010.

G. Carlsson, A. J. Zomorodian, A. Collins, and L. J. Guibas. Persistence barcodes for shapes. *Proceedings of the Eurographs/ACM SIGGRAPH Symposium on Geometry Processing*, pages 124–135, 2004.

A. Cayley. On contour and slope lines. *The London, Edinburgh, and Dublin Philosophical Magazine and Journal of Science*, 18(120):264–268, 1859.

J. Cerf. La stratification naturelle des espaces de fonctions différentiables réelles et le théoréme de la pseudo-isotopie. *Publications Mathématiques de l'Institut des Hautes Études Scientifiques*, 39(1):7–170, 1970.

C. A. Charalambides. *Enumerative Combinatorics*. Chapman and Hall/CRC, 1st edition, 2019.

F. Chazal, D. Cohen-Steiner, M. Glisse, L. J. Guibas, and S. Y. Oudot. Proximity of persistence modules and their diagrams. In *Proceedings of the 25th Annual Symposium on Computational Geometry*, pages 237–246, 2009.

W. Crawley-Boevey. Decomposition of pointwise finite-dimensional persistence modules. *Journal of Algebra and Its Applications*, 14(5):1550066, 2015.

J. Curry. The fiber of the persistence map for functions on the interval. *Journal of Applied and Computational Topology*, 2(3-4):301–321, 2018.

J. Curry and A. Patel. Classification of constructible cosheaves. arXiv:1603.01587, 2016.

M. d'Amico, P. Frosini, and C. Landi. Natural pseudo-distance and optimal matching between reduced size functions. *Acta Applicandae Mathematicae*, 109(2):527–554, 2010.

V. De Silva, E. Munch, and A. Patel. Categorified Reeb graphs. *Discrete & Computational Geometry*, 55(4):854–906, 2016.

B. Di Fabio and C. Landi. The edit distance for Reeb graphs of surfaces. *Discrete & Computational Geometry*, 55(2):423–461, 2016.

H. Edelsbrunner and J. Harer. *Computational Topology: An Introduction*. American Mathematical Society, 2010.

H. Edelsbrunner and D. Morozov. Persistent homology: Theory and practice. In *Proceedings of the European Congress of Mathematics*, pages 31–50. European Mathematical Society Publishing House, 2012.

H. Edelsbrunner, J. Harer, V. Natarajan, and V. Pascucci. Morse–Smale complexes for piecewise linear 3-manifolds. *Proceedings of the 19th ACM Symposium on Computational Geometry*, pages 361–370, 2003a.

H. Edelsbrunner, J. Harer, and A. Zomorodian. Hierarchical Morse–Smale complexes for piecewise linear 2-manifolds. *Discrete & Computational Geometry*, 30:87–107, 2003b.

P. C. Fishburn and W. T. Trotter. Geometric containment orders: A survey. *Order*, 15:167–182, 1999.

G. Fleitas. Classification of gradient-like flows on dimensions two and three. *Boletim da Sociedade Brasileira de Matemática - Bulletin/Brazilian Mathematical Society*, 6(2):155–183, 1975.

R. Ghrist. Barcodes: The persistent topology of data. *Bulletin of the American Mathematical Society*, 45(1):61–75, 2008.

C. Gutierrez and W. de Melo. The connected components of Morse–Smale vector fields on two manifolds. In P. J. and do Carmo M., editors, *Geometry and Topology*, volume 597, pages 230–251. Springer, Berlin, Heidelberg, 1977.

A. Hatcher and J. Wagoner. *Pseudo-isotopies of compact manifolds*, volume 6 of *Asterisque*. Société mathématique de France, Paris, 1973.

J. Helman and L. Hesselink. Representation and display of vector field topology in fluid flow data sets. *IEEE Computer*, 22(8):27–36, 1989.

A. Hofmann, M. Krufczik, D. W. Heermann, and M. Hausmann. Using persistent homology as a new approach for super-resolution localization microscopy data analysis and classification of γH2AX foci/clusters. *International Journal of Molecular Sciences*, 19(8):2263, 2018.

W. Kim and F. Memoli. Generalized persistence diagrams for persistence modules over posets. arXiv:1810.11517, 2018.

E. Kulinich. On topologically equivalent morse functions on surfaces. *Methods of Functional Analysis and Topology*, 4(01):59–64, 1998.

Y. Lee, S. D. Barthel, P. Dlotko, S. M. Moosavi, K. Hess, and B. Smit. High-throughput screening approach for nanoporous materials genome using topological data analysis: Application to zeolites. *Journal of Chemical Theory and Computation*, 14(8):4427–4437, 2018.

S. Lockwood and B. Krishnamoorthy. Topological features in cancer gene expression data. *Biocomputing*, pages 108–119, 2015.

R. MacPherson and A. Patel. Persistent local systems. arXiv:1805.02539, 2018.

J. Martínez-Alfaro, I. S. Meza-Sarmiento, and R. Oliveira. Topological classification of simple Morse Bott functions on surfaces. In *Real and complex singularities*, volume 675, pages 165–179. American Mathematical Society, 2016.

Y. Matsumoto. *An Introduction to Morse Theory*. American Mathematical Society, 1997.

J. C. Maxwell. On hills and dales. *The London, Edinburgh, and Dublin Philosophical Magazine and Journal of Science*, 40(269):421–427, 1870.

J. Milnor. *Morse Theory*. Princeton University Press, New Jersey, NY, USA, 1963.

L. Nicolaescu. *An Invitation to Morse Theory*. Springer Verlag, 2007.

L. I. Nicolaescu. Counting Morse functions on the 2-sphere. *Compositio Mathematica*, 144(5):1081–1106, 2008.

A. A. Oshemkov and V. V. Sharko. Classification of Morse-Smale flows on two-dimensional manifolds. *Sbornik: Mathematics*, 189(8):1205–1250, 1998.

J. Palis and W. de Melo. *Geometric theory of dynamical systems*. Springer, 1982.

V. Pascucci and K. Cole-McLaughlin. Parallel computation of the topology of level sets. *Algorithmica*, 38(1):249–268, 2004.

M. Peixoto. On the classification of flows on 2-manifolds. In *Dynamical systems*, pages 389–419. Elsevier, 1973.

A. Poulenard, P. Skraba, and M. Ovsjanikov. Topological function optimization for continuous shape matching. *Computer Graphics Forum*, 37(5):13–25, 2018.

T. Qaiser, Y.-W. Tsang, D. Taniyama, N. Sakamoto, KazuakiNakane, D. Epstein, and N. Rajpoot. Fast and accurate tumor segmentation of histology

images using persistent homology and deep convolutional features. *Medical Image Analysis*, 55:1–14, 2019.

G. Reeb. Sur les points singuliers d'une forme de pfaff complètement intégrable ou d'une fonction numérique. *Comptes Rendus de l'Acadèmie des Sciences de Paris*, 222:847–849, 1946.

S. Roman. *Lattices and ordered sets*. Springer Science & Business Media, 2008.

T. Sakajo and T. Yokoyama. Tree representations of streamline topologies of structurally stable 2D incompressible flows. *IMA Journal of Applied Mathematics*, 83(3):380–411, 2018.

E. R. Scheinerman and J. C. Wierman. On circle containment orders. *Order*, 4(4):315–318, 1988.

L. Seemann, J. Shulman, and G. H. Gunaratne. A robust topology-based algorithm for gene expression profiling. *ISRN Bioinformatics*, 2012(381023), 2012.

V. Sharko. On topological equivalence Morse functions on surfaces. In *International Conference at Chelyabinsk State University, Low-Dimensional Topology and Combinatorial Group Theory*, pages 19–23, 1996.

V. Sharko. Smooth and topological equivalence of functions on surfaces. *Ukrainian Mathematical Journal*, 55(5):832–846, 2003.

A. Szymczak. Hierarchy of stable Morse decompositions. *IEEE Transactions on Visualization and Computer Graphics*, 19(5):799–810, 2012.

K. Turner, S. Mukherjee, and D. M. Boyer. Persistent homology transform for modeling shapes and surfaces. *Information and Inference: A Journal of the IMA*, 3(4):310–344, 2014.

O. Veblen. Theory on plane curves in non-metrical analysis situs. *Transactions of the American Mathematical Society*, 6(1):83–98, 1905.

X. Wang. The C^*-algebras of Morse–Smale flows on two-manifolds. *Ergodic Theory and Dynamical Systems*, 10(3):565–597, 1990.

Y. Zhou, J. Lazovskis, M. J. Catanzaro, M. Zabka, and B. Wang. Persistence-driven design and visualization of Morse vector fields (poster and extended abstract). *China Visualization and Visual Analytics Conference*, 2019.